The Orbital Ground State of the Azide−Substrate Complex of Human Heme Oxygenase Is an Indicator of Distal H-Bonding: Implications for the Enzyme Mechanism[†]

Hiroshi Ogura,[‡] John P. Evans,[§] Dungeng Peng,[‡] James D. Satterlee,[||] Paul R. Ortiz de Montellano,[§] and Gerd N. La Mar*[,‡]

Department of Chemistry, University of California, Davis, California 95616, Department of Chemistry, Washington State University, Pullman, Washington 99163, and Department of Pharmaceutical Chemistry, University of California, 600 16th Street, San Francisco, California 94158-2517

Received December 27, 2008; Revised Manuscript Received February 19, 2009

ABSTRACT: The active site electronic structure of the azide complex of substrate-bound human heme oxygenase 1 (hHO) has been investigated by ^{1}H NMR spectroscopy to shed light on the orbital/spin ground state as an indicator of the unique distal pocket environment of the enzyme. Two-dimensional ^{1}H NMR assignments of the substrate and substrate-contact residue signals reveal a pattern of substrate methyl contact shifts that places the lone iron π-spin in the d_{xz} orbital, rather than the d_{yz} orbital found in the cyanide complex. Comparison of iron spin relaxivity, magnetic anisotropy, and magnetic susceptibilities argues for a low-spin, $(d_{xy})^2(d_{yz},d_{xz})^3$, ground state in both azide and cyanide complexes. The switch from singly occupied d_{yz} for the cyanide to d_{xz} for the azide complex of hHO is shown to be consistent with the orbital hole determined by the azide π-plane in the latter complex, which is ~90° in-plane rotated from that of the imidazole π-plane. The induction of the altered orbital ground state in the azide relative to the cyanide hHO complex, as well as the mean low-field bias of methyl hyperfine shifts and their paramagnetic relaxivity relative to those in globins, indicates that azide exerts a stronger ligand field in hHO than in the globins, or that the distal H-bonding to azide is weaker in hHO than in globins. The Asp140 → Ala hHO mutant that abolishes activity retains the unusual WT azide complex spin/orbital ground state. The relevance of our findings for other HO complexes and the HO mechanism is discussed.

Heme oxygenase (*1*−*3*) (HO)[1] is a nonmetal enzyme that uses protoheme (PH) as both a substrate and a cofactor to generate biliverdin, iron, and CO via three intermediates, mesohydroxyheme, verdoheme, and iron(III) biliverdin, as shown in Figure 1. The biliverdin product of the majority of HOs is further reduced to bilirubin by biliverdin reductase. In mammals, the ~300-residue enzyme is membrane-bound, and the three products have key roles as precursors to the antioxidant, bilirubin (*4*), in iron homeostasis (*5*), and as a potential neural messenger (*6*), respectively. A smaller (~200-residue) soluble HO is found in plants and photosynthetic bacteria (*7*), where the product biliverdin is converted to light-harvesting pigments, and in numerous pathogenic bacteria (*3, 8*−*10*), where its prime role is to secure iron from the host. While the HOs exhibit variable sequence homology (*9*), their structures exhibit a new, but remarkably conserved, α-helical fold (*11*−*16*). The distal HO pocket is unique in possessing a cluster of ordered water molecules organized within an extended H-bond network with some much stronger than usual H-bonds (*12, 13, 16*−*22*). Two prominent features of the HO reaction are that the ring cleavage is highly stereospecific (*3, 10, 23*) and that the ferryl species resulting from heterolytic O−O bond cleavage, which is responsible for oxidation by cytochromes P450 and peroxidases, is catalytically incompetent in HOs (*23*−*25*).

Control of heme stereoselectivity is rationalized by steric blocking by the distal helix of three of the meso positions, and the steric tilt or orientation of the exogenous ligand toward the fourth, unblocked position; differential stereoselectivity is determined primarily by differential heme seating in the active site (*2, 3, 10*−*16, 26, 27*). While the majority of HOs are α-meso-selective, the HO from the opportunistic pathogeneic bacterium *Pseudomonas aeruginosa* (*28*) (*Pa*HO) is unusual in that the product is a mixture of β- and δ-biliverdin. Initial mechanistic studies favored electrophilic attack on a meso position by Fe^{3+}-OOH (*3, 23*−*25*), but computational results suggested that this would involve an insurmountably high energy barrier and instead proposed (*29*−*31*) a tethered free radical mechanism in which the heme-bound O−O bond is homolytically cleaved. The destabilization of heterolytic O−O bond cleavage in HO has

[†] This research was supported by grants from the National Institutes of Health, GM62830 (G.N.L.M.) and DK30297 (P.R.O.d.M.).

* To whom correspondence should be addressed. E-mail: lamar@chem.ucdavis.edu. Phone: (530) 752-0958. Fax: (530) 7520-8995.

[‡] University of California, Davis.

[§] University of California, San Francisco.

[||] Washington State University.

[1] Abbreviations: HO, heme oxygenase; hHO, human heme oxygenase 1; *Pa*HO, *Pseudomonas aeruginosa* heme oxygenase; *Nm*HO, *Neisseria meningitidis* heme oxygenase; *Cd*HO, *Corynebacterium diphtheriae* heme oxygenase; PH, protohemin; DMDH, 2,4-dimethyldeuterohemin; DSS, 2,2-dimethyl-2-silapentane-5-sulfonate; NOESY, two-dimensional nuclear Overhauser spectroscopy; TOCSY, two-dimensional total correlation spectroscopy.

10.1021/bi802360g CCC: $40.75 © 2009 American Chemical Society
Published on Web 02/25/2009

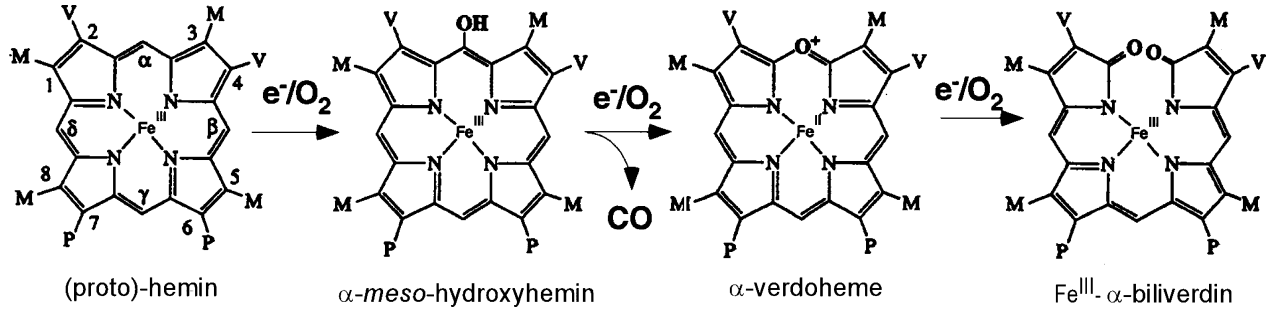

FIGURE 1: Sequence of intermediates in the heme oxygenase mechanism.

been attributed to H-bonding to the iron ligand by a set of conserved, ordered water molecules (*3, 12, 13, 16, 17, 29*−*31*). In the mammalian HO, these water molecules are H-bonded to distal Asp140 whose mutagenesis (*32, 33*) perturbs the ordered water molecule arrangement and abolishes HO activity, yielding the inactive ferryl unit.

The preference for homolytic over heterolytic O−O bond cleavage is unique to HOs, and early efforts were directed to searching for a unique spectroscopic signature of the active site of HOs that could be related to an active site environment distinct from those of the more common heme proteins. However, UV−visible, resonance Raman, EPR, and, until recently (*34, 35*), ^{1}H NMR spectra of HO complexes all were comparable to those for the same derivatives of a globin (*2, 36*−*42*). NMR spectra of paramagnetic hemoprotein derivatives provide unique information through their hyperfine shifts (*42, 43*) that reflect on functionally relevant structural information not readily gleaned from either crystal structures or other spectroscopic methods. Low-spin ferrihemoprotein complexes exhibit substrate contact shift patterns that reflect the pattern of delocalized spin density (*42, 43*). For the majority of $S = {}^1/_2$ ferrihemoproteins with relatively planar hemin, the lone spin resides in the π-bonding d_{yz} or d_{xz} orbital, which, for the geometry depicted in Figure 2A, can be delocalized into the symmetry-adapted $3e_\pi(yz)$ (spin distribution in Figure 3A) or $3e_\pi(xz)$ (spin distribution in Figure 3B) porphyrin molecular orbitals (*42, 44, 45*). For the extensively investigated His/CN$^-$-ligated ferrihemoproteins, the orbital ground state (singly occupied d_{xz} or d_{yz}) is determined by the axial His imidazole plane orientation (*44*), as defined by the angle ϕ_H relative to the porphyrin-based *x*-axis (Figure 2A). For α-meso-selective[2] HOs (i.e., with the substrate orientation depicted in Figure 2A), $\phi_H \sim 0$, and the lone spin in d_{yz} delocalizes into $3e_\pi(yz)$ with large predicted (*44*) and observed (*18, 19, 22, 41, 46*) contact shifts for porphyrin positions 2, 3, 6, and 7 (Figure 3).

Azide and cyanide complexes of ferriglobins exhibit very similar substrate contact shift patterns, and hence similar orbital ground states (*42*). It was, therefore, surprising that the azide complexes of both *Pa*HO and the HO from the pathogenic bacterium *Neisseria meningitidis* (*Nm*HO) exhibited (*34*) a switch between the two alternate orbital ground states (i.e., molecular orbitals in Figure 3), upon substituting azide for cyanide (*22, 28*), even though the axial His

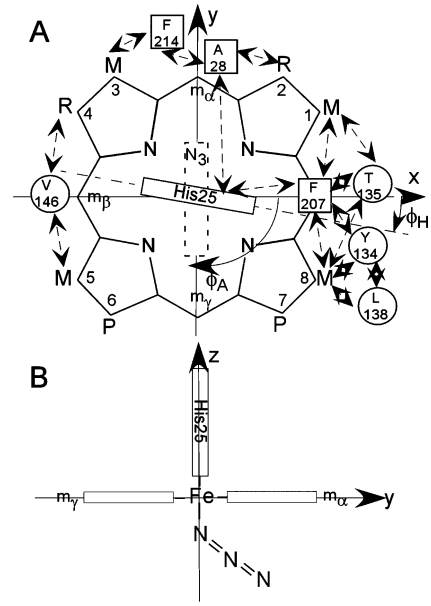

FIGURE 2: Structure of the (A) substrate, native protohemin (PH; R = vinyl), and 2-fold symmetric 2,4-dimethyldeuterohemin (DMDH; R = CH_3). The coordinate system for the iron d orbitals has the *x*- and *y*-axes passing through the β- and δ-meso positions (and the His25 imidazole plane) and the α- and γ-meso positions (azide π-plane), respectively, for the substrate orientation of the α-meso-selective hHO. The substrate contact residues are shown as squares and circles for proximal and distal residues, respectively. The orientations of the proximal His imidazole and distal azide π-planes are shown as solid and dashed rectangles, respectively; the angles between the *x*-axis and the proximal His imidazole and distal azide π-planes are ϕ_H and ϕ_A, respectively. Contacts expected from the crystal structures (*11, 13*) and observed by ^{1}H NMR for the WT hHO−DMDH−N_3 complex are shown by double-sided arrows. (B) Edge-on view from the positive *x*-axis that depicts the expected Fe−N_3 orientation, observed in the complex of rat HO (*62*).

imidazole orientation can be expected (*12, 14*) to be unchanged. On the basis of the failure of the correlation between the contact shift pattern and the His orientation in the azide complex, and supported by somewhat larger magnetic moments for the azide relative to cyanide complex, a novel $S = {}^3/_2$, $(d_{yz})^2(d_{xy})^1(d_{xz})^1(d_{z^2})^1$, rather than the common $S = {}^1/_2$, $(d_{xy})^2(d_{xz}d_{yz})^3$, ground state was proposed (*34*) for HO azide complexes. This unprecedented intermediate-spin ground state was attributed to a weaker than "normal" (i.e., globins) axial field strength for the azide complex. Since donation of an H-bond to the azide will weaken its ligand field, it was concluded (*34*) that the distal H-bonding to the ligand by the ordered water molecules in HOs is stronger than the H-bonding by distal basic side chains in globins. The interchange between the singly occupied d_{xz} and d_{yz} orbitals [with spin delocalization into $3e_\pi(xz)$ and $3e_\pi(yz)$,

[2] In the case of β (or δ)-meso-selective *Pa*HO, the substrate is rotated in plane (*15, 49*) ~90° relative to the conserved protein matrix and imidazole orientation compared to that depicted in Figure 2A, such that the unpaired d_{xz} spin is delocalized into $3e_\pi(xz)$ in the *Pa*HO−PH−CN complex, with predicted (*44*) and observed (*49*) large contact shifts for positions 1, 4, 5, and 8.

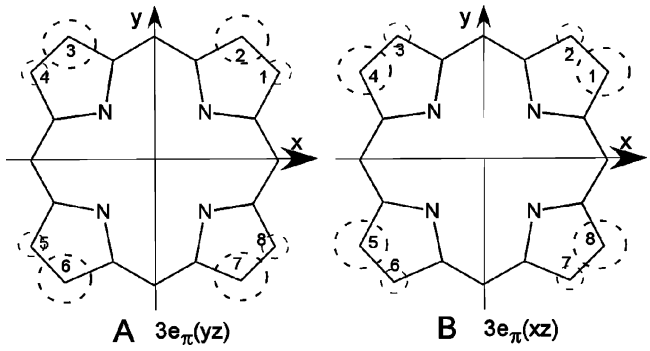

FIGURE 3: Symmetry-adapted substrate $3e_\pi$ molecular orbitals that illustrate the position of significant delocalized π-spin density on the substrate resulting from singly occupied metal−porphyrin π-bonding. The magnitude of the spin density, ρ_π, is shown by the size of the dashed circle. (A) $3e_\pi(yz)$, which interacts with only d_{yz} and results in large low-field methyl contact shifts for positions 2, 3, 6, and 7, as observed (*18*) for the cyanide complexes of α-meso-selective hHO, and (B) $3e_\pi(xz)$, which interacts with only d_{xz} and results in large low-field methyl contact shifts at positions 1, 4, 5, and 8, as observed in the azide complexes of α-meso-selective hHO. The orbitals in panels A and B are similarly occupied in all α-meso-selective HO cyanide (*18, 19, 22, 40, 41, 46*) and azide (*34, 35*) complexes, respectively.

respectively] between azide and cyanide complexes of HOs was suggested (*34*) as a feature diagnostic of a catalytically competent heme oxygenase active site. While a spectroscopic signature for HO activity would be very useful, it remains to be determined whether this proposed unique property, a switch in orbital ground states between the azide and cyanide complexes (*34*), is exhibited by all HOs and, if so, exactly what molecular/electronic structural feature is perturbed relative to other ferrihemoproteins with ostensibly conserved His/CN^- and His/N^-_3 chromophores, and how it relates to HO activity.

For the purpose of attempting to resolve some of these questions herein, we extend our ^{1}H NMR studies to the azide complex of human heme oxygenase 1 (hHO). Sequence homology between *Nm*HO and *Pa*HO is stronger (*9*) than that of either with hHO, particularly in the distal H-bond network, and it is of interest to compare the NMR properties of the azide complexes of hHO with those of *Nm*HO (*27, 34*) and *Pa*HO (*34*). Unfortunately, hHO in different complexes with the native substrate, protohemin (PH) (R = vinyl in Figure 2A), exhibits molecular heterogeneity (*40, 41, 47*) with respect to the orientation of PH about the α,γ-meso axis that reduces sensitivity and increases spectral overlap, which severely complicates assignments. Instead, we employ the 2-fold symmetric heme, 2,4-dimethyldeuterohemin (DMDH) (R = CH_3 in Figure 2A), which was found (*18*) to generate a single, homogeneous species in solution with a molecular structure essentially indistinguishable from that of the PH complex (*20, 47, 48*). To assess whether any NMR spectroscopic anomalies are related to the distinctive HO distal pocket environment that stabilizes hemolytic over heterolytic O−O bond scission, we include ^{1}H NMR data on the Asp140Ala point mutant, D140A-hHO−PH−N_3, which abolishes mammalian HO activity (*32, 33*) and instead favors heterolytic O−O bond cleavage.

We demonstrate that the switch between the alternate orbital ground states for the azide and cyanide complexes is apparently a general HO characteristic but that this orbital/spin state is retained in the inactive D140A-hHO−PH−N_3 mutant, indicating that this unusual property is not uniquely correlated with HO activity. These results allow us to formulate an alternate orbital/spin ground state for HO azide complexes that is consistent with differences in the π-bonding capability of N_3^- and CN^- and argue, contrary to previous proposals (*10, 34, 49*), for stronger, rather than weaker, azide field strength, and hence weaker rather than stronger H-bonding to the exogenous ligands in HOs than in globins.

EXPERIMENTAL PROCEDURES

Protein Sample. Solubilized, wild-type hHO and the point mutant D140A-hHO were prepared as reported previously (*24, 32*). 2,4-Dimethylprotoporphyrin IX (DMDH) (R = methyl in Figure 2A) was purchased from Mid-Century Chemicals and the iron inserted by standard procedures (*50*). The 1:1 molar equivalent of DMDH was titrated into apo-hHO in ^2H_2O in the presence of 20 mM KN_3 buffered by 50 mM phosphate (pH ~7.1).

NMR Spectroscopy. ^{1}H NMR data were collected on Bruker AVANCE 500 and 600 spectrometers operating at 500 and 600 MHz, respectively. Reference spectra were collected in ^2H_2O over the temperature range of 15−35 °C at both a repetition rate of 1 s^{-1} over a spectral width of 40 ppm and at 5 s^{-1} over a spectral width of 200 ppm. Chemical shifts are referenced to 2,2-dimethyl-2-silapentane-5-sulfonate (DSS) through the water resonance calibrated at each temperature. Nonselective T_1 values were determined by the standard inversion−recovery pulse sequence and estimated from the null point; 600 MHz NOESY spectra (*51*) (mixing time of 40 ms; repetition rate of 1−2.5 s^{-1}) and 500 MHz Clean-TOCSY spectra [to suppress the ROESY response (*52*); spin lock of 25 ms; repetition rate of 1−2 s^{-1}] were recorded over a bandwidth of 25 kHz (NOESY) and 12 kHz (TOCSY) using 512 t_1 blocks of 128 and 256 scans each consisting of 2048 t_2 points. Two-dimensional data sets were processed using Bruker XWIN on a Silicon Graphics Indigo workstation and consisted of 30° or 45° sine-squared bell apodization in both dimensions, with zero-filling to 2048 × 2048 data points prior to Fourier transformation.

Paramagnetic Susceptibility Comparison. Solution ^{1}H NMR (*53, 54*) was used to determine the difference in paramagnetic susceptibility, $\Delta\chi_M$

$$\Delta\chi_M = \chi_M(\text{hHO−DMDH−N}_3) - \chi_M(\text{hHO−DMDH−CN}) \quad (1)$$

between the accepted $S = {}^1/_2$ hHO−DMDH−CN complex and the hHO−DMDH−N_3 complex, to assess the potential population of an $S > {}^1/_2$ ground state for the latter complex. A 2.0 mM hHO−DMDH−H_2O solution 50 mM in phosphate (pH 7.1) (concentration determined with an ε of 140 mM^{-1} cm^{-1}), to which was added 10 mM dioxane,[3] was split into two samples. The first solution was diluted by 10% by volume with a phosphate-buffered ^1H_2O solution (pH 7.1) 400 mM in KN_3 to yield a 1.8 mM hHO−DMDH−N_3 solution in ^1H_2O. The second solution was diluted by 10%

[3] Both dioxane and *tert*-butanol were used as susceptibility markers. However, addition of *tert*-butanol significantly perturbed the hyperfine shift pattern of the azide complex, indicating specific interactions near the active site. Addition of dioxane left the ^{1}H NMR spectra of both the azide and cyanide complexes unperturbed.

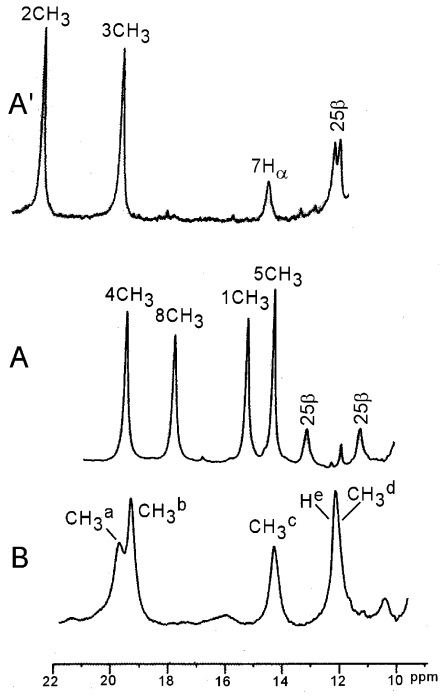

FIGURE 4: Resolved portions of the 600 MHz ^{1}H NMR spectra of (A) hHO−DMDH−N_3 and (B) D140A-hHO−DMDH−N_3 complexes. Panel A′ reproduces the same spectral portions for the hHO−DMDH−CN complex (*18*). All samples are at 30 °C in ^2H_2O, 50 mM in phosphate (pH 7.4). DMDH peaks are labeled by the Fisher notation (see Figure 3), and residue peaks are labeled by the residue number and its position within the residue.

by volume with a phosphate-buffered, 50%/50% (v:v) ^1H_2O/^2H_2O solution (pH 7.1), 400 mM in KCN, to yield a 1.8 mM hHO−DMDH−CN solution in 95% ^1H_2O and 5% ^2H_2O. The equimolar (1.8 mM) hHO−DMDH−CN and hHO−DMDH−N_3 solutions at identical ionic strengths were placed in the center tube and annulus of a concentric 5 mm NMR tube, and the chemical shift difference, $\Delta\delta$, was measured on a 600 MHz spectrometer at 25 and 35 °C. This difference in chemical shift is related to the difference in paramagnetic susceptibility between the cyanide and azide complex as given by (*53, 54*)

$$\Delta\delta = 10^3 M \Delta\chi_M/3 \quad (2)$$

Using the essentially invariant paramagnetic susceptibility for the established low-spin cyanide complex of ferric HO (*34*), χ_M(cyanide complex) $\sim 3.6 \times 10^{-8}$ m^3/mol, χ_M(hHO−DMDH−N_3) can be estimated, and the effective magnetic moment (μ_{eff}) for the azide complex can be determined by

$$\mu_{eff}(\text{hHO−DMDH−N}_3) = [3kT\chi_M(\text{hHO−DMDH−N}_3)/N_A\mu_o]^{1/2} \quad (3)$$

RESULTS

Spectral Comparison of N_3^- and CN^- Complexes. The strongly low-field, contact-shifted methyl resonances indicative of large π-spin density are resolved in the low-field portion of the ^{1}H NMR spectrum. The low-field resolved portion of the 600 MHz ^{1}H NMR reference spectrum of the hHO−DMDH−N_3 complex in ^2H_2O is shown in Figure 4A and can be compared to that of the hHO−DMDH−CN complex (*18*) in ^2H_2O in Figure 4A′. Assignments for the substrate resonances are given in the Fisher notation and for amino acid residues by residue number and position. Noteworthy is the observation (*18*) that the CN^- complex exhibits two resolved methyls, while the WT azide complex displays four methyls in this window. The nonselective T_1 values (not shown) for the resolved methyls of the hHO−DMDH−N_3 complex are ~85 ms, which is a factor of less than ~2 shorter than for the cyanide complex (*18, 41*). The $1CH_3$ and $8CH_3$ peaks of the hHO−DMDH−N_3 complex exhibit line broadening over those of the $4CH_3$ and $5CH_3$ peaks (in spite of similar T_1 values), which arises from rapid exchange (*55*) between alternate microenvironments at the substrate periphery. The two remaining methyls will be shown to appear within the diamagnetic envelope at 0−10 ppm. The DMDH methyl peaks to the low field of ~10 ppm, and to the high field of ~10 ppm, in the hHO−DMDH−N_3 complex exhibit very weak anti-Curie and markedly stronger anti-Curie behavior, respectively (not shown; see Figure S1 of the Supporting Information).

The low-field resolved portion of the NMR spectrum of the D140A-hHO−DMDH−N_3 complex in ^2H_2O is shown in Figure 4B. Spectra over a wide range of temperature (not shown; see Figure S2 of the Supporting Information) reveal four methyls, labeled CH_3^a−CH_3^d (intensity of approximately three protons), and a single proton peak, H^e, to the low field of ~10 ppm similar to that for the hHO−DMDH−N_3 complex. The T_1 values for the methyl resonances are similar (~80 ms) to those for the WT complex. The methyl peaks exhibit significant and differentially broadened resonances at 30 °C, which are broadened further at lower temperatures (not shown; see Figure S2 of the Supporting Information). This behavior indicates an exchange phenomenon, as observed for WT, but with a slower rate (*55*). Weak anti-Curie behavior is displayed by the low-field methyls in the D140A-hHO−DMDH−N_3 complex, similar to that observed for WT (not shown; see Figure S2 of the Supporting Information).

Assignment Protocols. We focus here only on the electronic structure of the chromophore, and hence, the only resonances of interest are those for DMDH and sufficient active site residues in contact with DMDH to associate each pyrrole with a specific protein environment in the heme pocket, as defined in the crystal structure (*13*). These limited but crucial assignments were optimally pursued in a ^2H_2O solution of the hHO−DMDH−N_3 complex. While the hHO azide crystal structure has not been reported, comparison of the rat HO azide crystal structure (*12*) with those of rat HO having numerous other ligands, including cyanide (*14*), show that heme contact residues are unchanged in the various derivatives. Our working hypothesis is that this is also true for hHO.

The DMDH assignments are assigned very straightforwardly by the pattern of inter-methyl and methyl-propionate $C_\alpha H$ NOESY cross-peaks about the substrate periphery, as reported for the hHO−DMDH−CN (*18*) and *Nm*HO−DMDH−N_3 (*46*) complexes. We note that DMDH, because of its 2-fold symmetry, does not possess unique labeling for each pyrrole substituent. However, we adopt the convention of numbering positions [as reported for the hHO−DMDH−CN complex (*18*)], which parallels that for the major solution isomer of hHO−PH (*41*), as depicted in Figure 2A. Active site residues are assigned by TOCSY detection of the spin

connectivity that uniquely identifies residue type, and by the NOESY contacts among these residues and between these residues and DMDH, as predicted by the crystal structure (*13*). The uniqueness of both scalar and dipolar connectivities is confirmed on the basis of two-dimensional experiments over a range of temperatures, where the natural temperature dependence of hyperfine shifts serves as a "third dimension" for editing the spectra. The expected, and observed, active site residue−substrate contacts are depicted schematically in Figure 2A. The assignments were greatly aided by the observation of very similar dipolar shifts for heme contact residues in the azide and the previously reported (*18*) cyanide complex. Moreover, hHO possesses an extended aromatic cluster on the distal side, conserved in both substrate-bound and substrate-free hHO (*13, 56*), that predicts and allows the observation of (*18*) highly characteristic NOESY cross-peak patterns among TOCSY-detected aromatic rings with characteristic low-field shifts, in a Phe95-Trp96-Phe47-Phe167-Leu164-Phe166-Tyr58 pattern.

Assignment of the WT hHO−DMDH−N_3 Complex. Portions of the 600 MHz ^{1}H NMR NOESY spectrum of the hHO−DMDH−N_3 complex in ^2H_2O illustrating the key contacts about the DMDH periphery in the order $C_\alpha H$-CH_3-CH_3-CH_3-CH_3-CH_3-CH_3-$C_\alpha H$, with weak cross-peaks between the outer and central methyl pairs and moderate cross-peaks between the other two methyl pairs, are shown by arrows in Figure 5. Key DMDH−residue and inter-residue dipolar contacts are illustrated in both Figures 5 and 6. A pair of strongly low-field shifted and relaxed geminal protons can arise only from the remaining heme ligand, His25 C_βHs (Figure 6C,D,F).

The NOESY cross-peak of an Ala methyl to His25 $C_\alpha H$ (Figure 6B), together with the Ala methyl NOESY cross-peask to an upfield DMDH methyl (Figure 6B), uniquely identifies Ala28 and assigns $2CH_3$ and $3CH_3$. Ala28 $C_\beta H_3$ NOESY cross-peaks to a Phe ring and to $2CH_3$ (Figure 6B) uniquely identify Phe214, while an Ala28 $C_\beta H_3$ cross-peak to another aromatic ring (Figure 6B) that exhibits cross-peaks to $1CH_3$ (Figure 6A) and $8CH_3$ (Figure 5E) uniquely locates the ring of Phe207. NOESY cross-peaks of a Thr to both $8CH_3$ (Figure 5A) and $1CH_3$ (Figure 5B) and a cross-peak between an aromatic ring and both $8CH_3$ (Figure 5E) and Phe207 (Figure 6E) uniquely locate Thr135 and Tyr134. The methyls of a Val exhibit contacts to both $4CH_3$ (Figure 5A) and $5CH_3$ (Figure 5B) that can arise from only Val146. The expected and observed heme pocket contacts are depicted schematically in Figure 2A, and chemical shifts of DMDH and heme contact residues are provided in Table 1. Lastly, characteristic NOESY cross-peaks among weak to moderately dipolar-shifted rings in the aromatic cluster identify six additional aromatic (Phe47, -95, -166, and -167, Tyr58, and Trp96) and part of one aliphatic (Leu164) residue with shifts listed in the Supporting Information.

The large hyperfine shifts for the hHO−DMDH−N_3 methyls at positions 1, 4, 5, and 8 dictate single occupancy of d_{xz}, with spin delocalized into $3e_\pi(xz)$ (Figure 3A), as observed (*34*) for the *Nm*HO−PH−N_3 complex (*34*). The active site residues, on the other hand, exhibit dipolar shifts very similar to those of the CN^- complex (*18*) whose d_{yz} orbital [with spin delocalization into $3e_\pi(yz)$ (Figure 3B)] is singly occupied (see Table 1 and Table S1 of the Supporting Information).

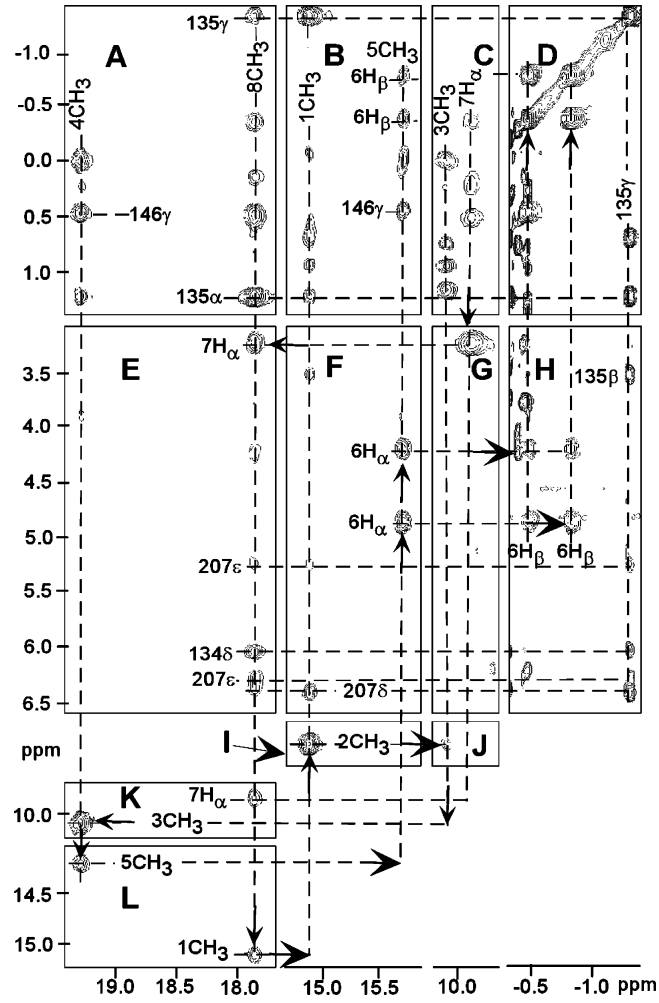

FIGURE 5: Portions of the 600 MHz ^{1}H NMR NOESY spectrum (mixing time of 40 ms, repetition rate of 2.5 s^{-1}, sweep width of 35 ppm) of the hHO−DMDH−N_3 complex in ^2H_2O, 50 mM in phosphate (pH 7.4), at 30 °C, illustrating the dipolar contacts about the DMDH perimeter, as shown by arrows (A−L). Key residue−DMDH and inter-residue contacts are from Val146 to $4CH_3$ (A) and $5CH_3$ (B), from Thr135 to $8CH_3$ (C) and $1CH_3$ (D), from Phe207 to $8CH_3$ (E) and $1CH_3$ (F), from the Tyr134 ring to $8CH_3$ (E), and from Thr135 to $C_\gamma H_3$ (H).

Assignments in D140A-hHO−DMDH−N_3. The methyls on a given pyrrole exhibit very sizable NOESY cross-peaks and numerous common cross-peaks to pyrrole contact residues. Two methyls adjacent to the same meso-H exhibit only a very small inter-methyl cross peak but still exhibit common cross-peaks to the same heme contact residue. Variable-temperature NMR spectra of the hHO−DMDH−N_3 complex identify four resolved methyl peaks and one resolved single-proton peak H^e (not shown; see Figure S2 of the Supporting Information). The much larger line widths, lower concentration (∼1.5 mM), and hence strongly reduced sensitivity relative to the WT complex preclude the detection of the weak NOESY cross-peak within the methyl pairs on adjacent pyrroles, $1CH_3/8CH_3$ and $4CH_3/5CH_3$, but should readily allow the detection of the moderate-intensity cross-peak within methyl pairs on the same pyrrole, $1CH_3/2CH_3$ and $3CH_3/4CH_3$. The excessive line width, moreover, precludes the detection of the intraresidue TOCSY cross-peaks for DMDH contact residues. However, one qualitative conclusion is that there are still four low-field DMDH methyls, as in the WT hHO−DMDH−N_3 complex, and not

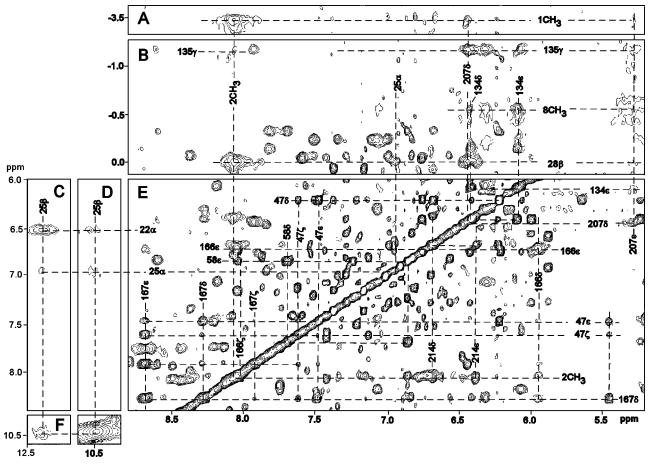

FIGURE 6: Portions of the 600 MHZ ^{1}H NMR NOESY spectrum (mixing time of 40 ms, repetition rate of 1.5 s^{-1}, sweep width of 17 ppm) illustrating key DMDH−residue and inter-residue contacts: (A) from $1CH_3$ to the Phe207 ring, (B) from $8CH_3$ to the Tyr134 ring, from Ala28 $C_\beta H_3$ to the Phe207 ring and His25 $C_\alpha H$, (C, D, and F) His25 intraresidue, (E) from $2CH_3$ to the Phe214 ring, and (E) interaromatic and aromatic−aliphatic contacts involving Phe47, Tyr58, Tyr134, Phe166, Phe167, and Leu164 in the distal aromatic cluster. Note that in panel B, $1CH_3$ and $8CH_3$ are folded in.

Table 1: Chemical Shifts for DMDH and Key Active Site Residues for DMDH−Azide Complexes of WT hHO and D140A-hHO

	WT hHO		D140A-hHO	
residue	proton	azide[a]	cyanide[b]	azide[a]
DMDH	$1CH_3$	15.09	8.95	19.9
	$2CH_3$	7.71	21.37	
	$3CH_3$	10.07	18.25	
	$4CH_3$	19.34	8.51	19.4/14.5[c]
	$5CH_3$	14.27	9.78	14.5/19.4[c]
	$6C_\alpha H$	4.20	11.02	
	$6C_\alpha H'$	4.85	10.24	
	$6C_\beta H$	−3.90	−0.05	
	$6C_\beta H'$	−7.50	0.12	
	$7C_\alpha H$	3.24	13.13	
	$7C_\alpha H'$	9.84	7.02	
	$8CH_3$	17.78	8.29	12.4
Arg22	$C_\alpha H$	6.67	6.27	6.21
His25	$C_{\beta 1} H$	10.78	8.95	9.3
	$C_{\beta 2} H$	12.68	10.75	12.3
Ala28	$C_\alpha H$	3.40	2.42	
	$C_\beta H_3$	−0.07	−2.14	
Tyr134	$C_\delta Hs$	6.37	6.56	6.55
	$C_\varepsilon Hs$	6.05	6.25	6.13
Thr135	$C_\alpha H$	1.23	2.39	2.36
	$C_\beta H$	3.75	3.35	3.55
	$C_\delta H_3$	−1.31	−0.10	0.07
Leu138	$C_\alpha H$	3.76	3.12	−
	$C_\beta Hs$	−0.35, 0.47	−0.40, 0.55	−
	$C_\delta H$	0.48	0.55	−
Val146	$C_\alpha H$	3.88	3.76	
	$C_\beta H$	2.26	2.32	
	$C_\gamma H_3$	0.51	0.56	
	$C_\gamma H_3'$	0.47	0.71	
Phe207	$C_\delta Hs$	6.43	6.43	−
	$C_\varepsilon Hs$	5.25	5.82	−
Phe214	$C_\delta Hs$	6.80	6.67	−
	$C_\varepsilon Hs$	6.35	6.35	−
	$C_\zeta H$	6.27	6.45	−

[a] Chemical shift in parts per million referenced to DSS via the residual solvent signals, in ^2H_2O, 50 mM in phosphate (pH 7.1), at 30 °C. [b] Chemical shift in parts per million referenced to DSS in ^1H_2O, 50 mM in phosphate. Data from ref *18*. [c] The $4CH_3$ and $5CH_3$ assignments could not be differentiated.

two, as in the hHO−DMDH−CN complex (*18*), indicating that the singly occupied d_{xz} orbital is retained in the mutant azide complex.

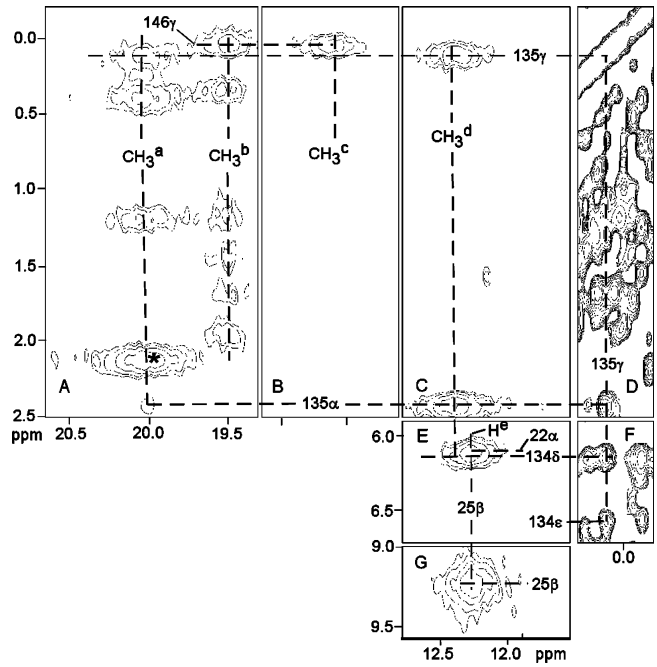

FIGURE 7: Portion of the 600 MHZ ^{1}H NMR NOESY spectrum (mixing time of 40 ms, repetition rate of 25 s^{-1}) of the D140A-hHO−DMDH−N_3 complex in ^2H_2O, 100 mM in phosphate (pH 7.1), at 30 °C illustrating the DMDH contacts to the four low-field resolved methyls labeled M_a−M_d to key active site residues (A−C, E, and F), as well as key intraresidue Thr135 contacts (D), Thr135−Tyr134 contacts (F), and both inter-residue His25 (G) and His25−Lys22 contacts (E). The peak marked with an asterisk possibly arises from $2CH_3$.

Portions of the NOESY spectrum of the D140A-hHO−DMDH−N_3 complex in ^2H_2O containing the low-field methyl resonances are shown in Figure 7. The absence of cross-peaks between well-separated low-field methyl peaks excludes any of these pairs arising from methyls of the same pyrrole. The near degeneracy of CH_3^a and CH_3^b prevents detection of even a moderate-intensity NOESY cross-peak between them; however, the absence of any common cross-peaks to CH_3^a and CH_3^b over a range of temperatures similarly discounts their positions either on the same pyrrole or adjacent to the same meso position. Methyl peaks CH_3^a (Figure 7A) and CH_3^d (Figure 7C) exhibit common NOESY cross-peaks to an aliphatic and aromatic residue, indicating aliphatic−aromatic residue contacts (Figure 7D,F) that are very similar in pattern to those observed in the hHO−DMDH−N_3 complex for $1CH_3$ and $8CH_3$ with Thr135 and Tyr134, respectively, and are so assigned. Methyl peaks CH_3^b (Figure 7A) and CH_3^c (Figure 7B) exhibit a common NOESY cross-peak to an upfield-shifted methyl in a manner similar to that observed in the hHO−DMDH−N_3 complex for $4CH_3$ (Figure 5A) and $5CH_3$ (Figure 5B) with Val146 and are so assigned; the two methyls could not be differentiated. Thus, the same four methyl peaks appear in the low-field resolved spectral window for both the WT azide and D140A mutant azide complexes. The intense NOESY cross-peak for peak H^e is consistent with it arising from the His25 $C_\beta Hs$ (Figure 7G). The logical conclusion from this similarity of the NOESY pattern between the mutant and WT proteins is that they display highly conserved active site structures. This is further supported by the observation of very similar NOESY cross-peaks among TOCSY-detected rings in the

distal aromatic cluster of both proteins (not shown; see the Supporting Information).

Comparison of Magnetic Susceptibilities of hHO−DMDH−N_3 and hHO−DMDH−CN Complexes. The splitting of the dioxane signal, $\Delta\delta$, is measured as 2.8 ± 0.1 Hz at 25 °C and 3.1 ± 0.1 Hz at 35 °C, with the azide complex exhibiting the larger χ_M. The $\Delta\delta$ at 25 °C leads to a $\Delta\chi_M$ of 0.81×10^{-8} m^3/mol via eqs 1 and 2. The χ_M value for the low-spin, cyanide complex of HO (*34*) indicates χ_M(hHO−DMDH−CN) $\sim 3.6 \times 10^{-8}$ m^3/mol, such that we obtain a χ_M(hHO−DMDH−N_3) of $\sim 4.4 \times 10^{-8}$ m^3/mol. Equation 3 yields a μ_{eff}(hHO−DMDH−CN) of ~2.6 μ_B and a μ_{eff}(hHO−DMDH−N_3) of ~2.9 μ_B at 25 °C. Clearly, χ_M and μ_{eff} for the azide complex are only very modestly increased (~20 and ~10%, respectively) over those for the cyanide complex.

DISCUSSION

Active Site Molecular Structure of the Wild-Type Azide Complex. The observation of all of the contacts between active site residues and the individual methyls of DMDH expected on the basis of both the crystal structure (*13*) and the solution structure of the cyanide complex (*18*) confirms an essentially conserved active site structure for the WT azide complex. This is further supported by the observation of the dipolar contacts among numerous rings in the aromatic cluster of the distal side of the substrate. Crystal structures of the azide and cyanide complexes of the highly homologous rat HO complex have already demonstrated (*12, 14*) that the active site structure is highly conserved.

The pattern of DMDH hyperfine shifts has clearly shown (*18*) that d_{yz} [with spin delocalization into $3e_\pi(yz)$ (Figure 3A)] is singly occupied for the hHO−DMDH−CN complex. The pattern of DMDH methyl hyperfine shifts for the hHO−DMDH−N_3 complex, large low-field contact-dominated hyperfine shifts for $1CH_3$, $4CH_3$, $5CH_3$, and $8CH_3$, is consistent with only single-spin occupation of d_{xz} [with spin delocalized into $3e_\pi(xz)$ (Figure 3B)]. This further confirms the original observation (*34*) of the switch of the orbital grounds states between the azide and cyanide complexes of *Pa*HO and *Nm*HO and supports the notion that this switch may be diagnostic of the active site structure of HOs. For both the *Pa*HO and *Nm*HO complexes, it was proposed (*34*), on the basis of the assumption that only the axial His orientation can control the orbital ground state (*44*), that the singly occupied d_{xz} (d_{yz}) for α-meso (β,δ-meso)-selective HOs can arise only with the unusual $S = {}^3/_2$, $(d_{yz})^2(d_{xz})^1(d_{xy})^1(d_{z^2})^1$ [$(d_{xz})^2(d_{yz})^1(d_{xy})^1(d_{z^2})^1$] ground state. To determine the orbital/spin state consistent with the present ^{1}H NMR data on the DMDH azide complex of α-meso-selective hHO, we will consider separately the spin and orbital parts.

hHO−DMDH−N_3 Possesses an $S = {}^1/_2$, Rather Than an $S = {}^3/_2$, Ground State. An $S = {}^3/_2$ ground state was postulated (*34*) for bacterial HOs primarily on the basis of a switch between d_{yz} and d_{xz} single-spin occupation in azide and cyanide complexes of *Pa*HO and *Nm*HO that is completely inconsistent with the expected conserved axial His orientation, and the finding that the magnetic susceptibility in the *Pa*HO−PH−N_3 complex was twice that for the $S = {}^1/_2$ cyanide complex. In contrast, we conclude that the spin ground state for the hHO−DMDH−N_3 complex is $S = {}^1/_2$, as in the hHO−DMDH−CN complex (*18*), for four reasons. (1) Nuclear T_1 values, and hence electronic T_1 values (*57*), are within a factor of 2 for azide and cyanide complexes and highly characteristic of $S = {}^1/_2$ ferric hemoproteins (*42, 43, 57*). (2) The dispersion of chemical shifts for nonligated residues, which arises from dipolar shifts due to anisotropy of the paramagnetic susceptibility tensor (*42, 43*), is very large and essentially the same in hHO−DMDH−N_3 and hHO−DMDH−CN complexes, as evidenced by the very similar shift magnitude and shift pattern for nonligated residues in the cyanide and azide complexes (Table 1). (3) Most directly, the magnetic susceptibility difference between the azide and cyanide complexes of hHO is only $\sim 0.8 \times 10^{-8}$ m^3/mol, which, with the reported χ_M of $\sim 3.6 \times 10^{-8}$ m^3/mol for an HO cyanide complex (*34*), indicates an only ~20% increase in χ_M for the azide over the cyanide complex and this difference is a factor ~5 smaller than the reported difference in χ_M for the same pair of *Pa*HO complexes (*34*). The small increase in the μ_{eff} of the azide, ~2.9 μ_B, over that of the cyanide (~2.6 μ_B) is much smaller than expected even for a spin-only $S = {}^3/_2$ ground state. The very modest increase in $\Delta\chi_M$ at elevated temperatures, as well as the weak anti-Curie behavior of the hHO−DMDH−N_3 methyl hyperfine shifts (not shown; see Figure S1 of the Supporting Information), is in complete accord with an $S = {}^1/_2$ ground state and a very modest thermal population of the $S = {}^5/_2$ excited state, which is commonly found in globin azide derivatives (*42, 58, 59*). (4) Lastly, and very importantly, as shown below, a robust interpretation can be offered for the switch of the singly occupied d_π orbital of d_{yz} in the hHO−DMDH−CN complex to d_{xz} in the hHO−DMDH−N_3 complex within the $S = {}^1/_2$ ground state that is completely consistent with the expected conservation of the axial His orientation and the π-bonding properties of ligated azide. It is noted that EPR data at cryogenic temperatures on the azide complex of rat HO have also been interpreted as arising from a low-spin state with eclipsed axial ligand planes (*60*).

The Axial Field Strength Is Stronger in hHO Than in Globin Azide Complexes. ^{1}H NMR studies of azide complexes of globins have been interpreted (*42, 59*) on the basis of an $S = {}^1/_2 \leftrightarrow S = {}^5/_2$ equilibrium (*58*), with the low-field bias of the methyl shifts and the degree of anti-Curie behavior indicative of the degree of high-spin population. The azide complexes of globins are qualitatively differentiated from those of HOs in that their low-field methyl shifts are greater and the degree of their anti-Curie behavior is larger. Hence, the lower $S = {}^5/_2$ population for hHO than for globins dictates a stronger axial field strength in the azide complexes of hHO than in complexes of the globins. Magnetic resonance studies have shown that the axial anisotropy increases and the electronic T_1 decreases (nuclear T_1 increases), with an increasing axial field strength in an $S = {}^1/_2$ ferrihemin or ferrihemoprotein (*42, 45*). The methyl T_1 values and dipolar shift dispersion that relate to the magnitude of the magnetic anisotropy are also much larger in hHO than in globin azide complexes, confirming a stronger axial field in the HO complexes. The nature of the Fe−His bonding in HOs has been concluded (*37, 39, 61*) to be "normal" and not detectably differentiated from that in globins. Hence, the greater azide axial field strength in hHO versus that in globin

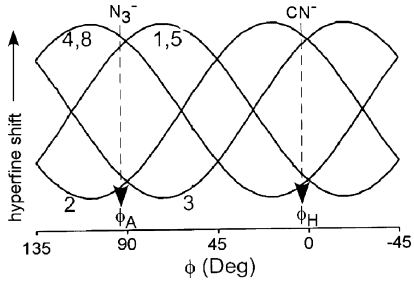

FIGURE 8: Empirical plot of DMDH methyl shifts as a function of the angle ϕ between the unique π-plane of the axial ligand that serves as the stronger π-donor to the iron in an $S = {}^1/_2$, $(d_{xy})^2(d_{xz},d_{yz})^3$ ferrihemoprotein (*27, 44*). The angle, ϕ, is defined in Figure 2A. The pattern of the observed DMDH methyl shifts, and the corresponding ϕ, are indicated by vertical arrows under CN^- (for the cyanide complex) and under N_3^- (for the azide complex).

complexes must result from a stronger bonding of the azide ligand in hHO than in globins.

The $(d_{xy})^2(d_{xz})^2(d_{xz})$ Orbital Ground State in hHO−DMDH−N_3 Is Determined by the Azide Orientation. The pattern of large low-field DMDH $1CH_3$, $4CH_3$, $5CH_3$, and $8CH_3$ contact shifts dictates a singly occupied d_{xz} that yields the delocalized spin in $3e_\pi(xz)$ (shown in Figure 3B), and it remains to be shown that this not only is consistent with the expected molecular structure (*62*) of the azide complex but also can be reasonably anticipated with the presently established larger azide axial field strength in HO than in globin complexes. The pattern of DMDH methyl hyperfine shifts as a function of the axial His orientation, given by the angle ϕ_H (shown in Figure 2A), has been empirically predicted (*44*) and gives rise to the pattern illustrated (*27*) in Figure 8. However, this plot can be generalized to represent the DMDH methyl shifts as a function of the angle, ϕ, to the unique π-plane of whichever axial ligand serves as the stronger π-donor to the iron. For His/CN^- ligation, the axial symmetry of the ligated cyanide necessarily leads to control of the orbital ground state by the axial histidine plane (ϕ_H in Figure 2A) (*42, 44*). The methyl shift pattern for the hHO−DMDH−CN complex has been reported previously (*18*) with contact shift magnitudes in the following order: $3CH_3 \sim 2CH_3 > 8CH_3 \sim 5CH_3 \sim 4CH_3 \sim 1CH_3$, which dictates a ϕ of ~0° in Figure 8 (vertical arrow under CN^-), in reasonable agreement with the crystallographic ϕ_H of ~0 (Figure 2A) (*13*).

When there are two non-axially symmetric ligands, the orbital ground state will depend on which of the two ligands serves as the stronger π-donor to the iron. In formulating (*34*) the $S = {}^3/_2$ ground state for the azide complex of *Nm*HO and *Pa*HO to account for the switch between the two π-orbitals in Figure 3 for the azide and cyanide complexes, the possible contribution of azide π-bonding to the orbital ground state was discounted on the basis of the axial symmetry of the azide ion. However, while the azide is axially symmetric, upon coordination to iron, the axial symmetry is broken and contributes a single π-system with well-defined orientation relative to the heme. An orientation of the azide terminus toward the α-meso position (i.e., as depicted in Figure 2B) in hHO can be reasonably expected since the bound NO in the hHO−PH−NO complex is sterically constrained to orient toward the α-meso position (*13*) as part of the stereoselectivity mechanism. The crystal structure of the azide complex reported for the highly homologous rat HO complex (*12*) shows the bent Fe−N_3

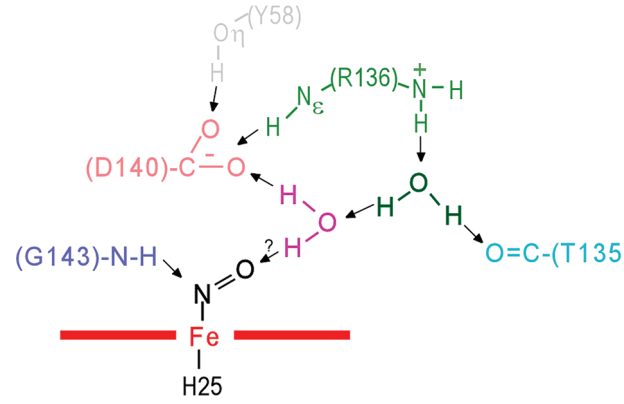

FIGURE 9: Schematic of active site structural features for the crystal structures (*13*) of the WT hHO−PH−NO complex, illustrating the relative positions of five key residues in the distal H-bonding network, Tyr58 (gray), Thr135 (aqua), Arg136 (light green), Asp140 (pink), and Gly143 (light blue), as well as two nonligated, ordered water molecules, water 1 (magenta) and water 2 (dark green) (*13*). The most significant structural difference in the D140A-hHO mutant is the replacement of the Asp140 carboxylate with a new water molecule. H-Bonds are shown as arrows.

unit directed toward the α-meso position as depicted in Figure 2B. The presently observed methyl shift pattern for hHO-DMDH-N_3 is as follows: $1CH_3 \sim 4CH_3 \sim 5CH_3 \sim 8CH_3 > 2CH_3 \sim 3CH_3$, which indicates a $\tilde{\phi}$ of 90° from Figur 8 (vertical arrow under N_3^-). This ϕ is precisely that expected for the orientation of the azide π-system (ϕ_A in Figure 2). Thus, it is the azide π-bonding that determines the orbital ground state in the azide complex of hHO, and the logical conclusion that follows is that the azide must be a better π-donor (stronger field) than the His imidazole in hHO.

Comparison of the Axial Field in HO and Globin Azide Complexes. The question of whether the azide axial field strength is generally stronger than for the His imidazole or whether this occurs in only HOs arises. The heme methyl ^1H NMR assignments of both the cyanide and azide complexes have been reported for globins (*42*), and while the low-field bias of the heme methyls at the same ambient temperature is always larger in the azide complexes than in the cyanide complexes, the pattern of shifts for the cyanide and azide complexes is very similar, with the following low-field shift magnitudes: $5CH_3 > 1CH_3 > 8CH_3 > 3CH_3$. This suggests that the imidazole π-bonding controls the orbital ground state in both cyanide and azide complexes of globins or that azide is a weaker π-donor than the axial His imidazole in globins. It should be noted that, once it is recognized that the orbital ground state in the hHO−DMDH−N_3 complex is determined by the azide, rather than the imidazole π-plane orientation, as in globins, the conclusion that azide exerts a stronger ligand field in HOs than globins follows directly.

Correlation between Azide Ligand Field Strength and Distal H-Bonding. The ligand field strength of azide can be modulated by distal H-bonding, with proton donation to either N_1 or N_3 resulting in weaker Fe−N_1 bonding (axial field strength). Hence, the stronger ligand field of the azide in HO than globins indicates that the distal H-bonding to the azide is weaker in hHO than in globins. The key distal H-bond interactions that involve the exogenous ligand, Tyr58, Thr135, Arg136, Gly143, and Asp140, and two ordered water molecules, water 1 (magenta) and water 2 (dark green), in the WT hHO−PH−NO complex (*13*), are depicted in Figure 9. Since water 1 must serve as a donor to the strong Asp140 carboxylate

acceptor, it is unlikely to serve as a significant H-bond donor to the iron ligand. A similar pocket structure can be assumed for the azide hHO complex. Thus, water 1 and the Gly143 NH group appear to provide H-bonds to the axial ligand much weaker than those provided by the generally basic residues in the distal pocket of globins (*63*).

Relevance to Other Studies. The ground states for *Pa*HO (*Nm*HO) azide complexes have been proposed (*34*) as $S = {}^3/_2$, $(d_{yz})^2(d_{xy})^1(d_{xz})^1(d_{z^2})^1$ [$S = {}^3/_2$, $(d_{xz})^2(d_{xy})^1(d_{yz})^1(d_{z^2})^1$] on the basis of the failure of the substrate methyl contact shifts to correlate with the axial His imidazole orientation and supported by a significant elevation of χ_M of the azide over the cyanide complexes. The arguments presented above obviate the first point. The fact that both *Nm*HO and *Pa*HO exhibit a switch between the alternate singly occupied d_{xz} and d_{yz} orbitals for the azide (*34*) and cyanide (*22, 28*) complexes in a manner very similar to that presently observed for hHO suggests a common $S = {}^1/_2$ ground state for both azide and cyanide complexes of HOs in general and dictates that the orbital ground state is similarly controlled in the azide complexes of all HOs. The larger increase in χ_M in the azide versus that in the cyanide complex (*34*) for the bacterial HOs versus the hHO complexes likely arises from a larger population of the excited $S = {}^5/_2$ state in the bacterial HOs. Consistent with this conclusion, the mean low-field methyl hyperfine shifts in *Nm*HO and *Pa*HO azide complexes are larger than in the hHO complex, and the methyl T_1 values are larger in hHO (~85 ms) than in bacterial HO [~40 ms (*35*)] azide complexes. Hence, the weaker azide field strength in bacterial relative to mammalian HO indicates stronger distal H-bonding to the azide in either *Pa*HO or *Nm*HO than in hHO.

Implications for the HO Mechanism. On the basis of the fact that hydrogen peroxide and ethyl peroxide yield α-meso-hydroxy- and α-meso-ethoxyhemin, respectively (*24, 25*), and the ENDOR detection (*64*) of the catalytically competent Fe^{3+}-OOH at cryo-temperatures upon radiolysis of the oxy complex, the mechanism (*2, 3*) of reaction was proposed to result from electrophilic attack on the α-meso carbon by the intact Fe^{3+}-OOH. Computational results (*29*) and interpretation of NMR data (*10*) have argued for a free radical mechanism, in which the hydroxyl radical resulting from homolytic O−O bond scission is tethered to the ordered water molecule cluster over the meso position that is attacked (*31*). A radical mechanism is supported by recent studies of electrophilic versus free radical reactions with heme in horseradish peroxidase (*65*).

An argument for the free radical mechanism has been advanced (*10, 34, 49, 66*) on the basis of a proposed substrate "self-activation" for free radical attack at a meso position due to single-spin population of the d_{xy} orbital that leads to ruffling of the porphyrin and significant π-spin delocalization to the meso positions. The rationale for proposing the single-spin population of d_{xy} was based on the premise that the exogenous ligand [directly proposed for azide (*34*) and hydroxide (*49*), and inferred for hydroperoxide (*10*)] exerts a significantly weakened axial field in HOs relative to that in globins and that this weakened axial field in HOs results from stronger distal H-bonding to the ligand in HOs than in globins. The weaker than "normal" (i.e., globins) axial field strength of hydroxide and azide in HO was attributed to strong distal H-bond donation by ordered water molecules. The ^{1}H NMR data for hHO presented here do not directly bear on the viability of the free radical mechanism but do not confirm the premise that the axial field strength of the exogenous ligand is weaker in HOs than globins. To disfavor the heterolytic O−O bond cleavage in the Fe^{3+}-OOH complexes of the globins, a weaker distal H-bond to azide in HOs than in globins might be reasonably expected and is confirmed here. Consistent with these findings, EPR data on the hydroperoxy complex of rat HO have been interpreted on the basis of the conventional d_π ground state (*60*) rather than the d_{xy} ground state predicted (*10, 49*) on the basis of strong distal H-bonding.

Influence of the Asp140 → Ala Mutation. The switch in the $S = {}^1/_2$ orbital ground state for cyanide and azide complexes may be diagnostic of the stronger-than-normal azide ligand field in HOs in general, but it clearly does not correlate with HO activity, inasmuch as the azide complex of inactive (*32*) D140A-hHO similarly exhibits[4] four low-field methyls with T_1 values similar to those in the hHO−DMDH−N_3 complex and similar weak anti-Curie behavior indicative of single occupation of the d_{xz} orbital as for the hHO−DMDH−N_3 complex. The crystal structure of the D140A-hHO−PH−NO complex has shown (*13*) that the most significant structural difference between the WT and the mutant is that a new ordered water molecule (water 3) replaces the carboxylate group of Asp140. Most importantly, the position of water 1 relative to the ligand remains approximately the same. However, the replacement of the strong H-bond acceptor carboxylate of Asp140 in the D140A-hHO mutant with a water molecule (water 3) makes water 1 a better H-bond donor to the ligand. The greater H-bond donation to the ligand by water 1 in the mutant is sufficient to accelerate heterolytic O−O bond cleavage, but insufficient to make the ligated azide a poorer H-bond donor than the His imidazole, hence the retention of the $S = {}^1/_2$, $(d_{xy})^2(d_{yz})^2(d_{xz})^1$ ground state.

The very delicate balance between the donor strength of the ordered water molecule (water 1) in the discrimination between the rate of homolytic and heterolytic O−O bond cleavage is indicated by a recent study of HO from *Corynebacteria diphtheriae* (*Cd*HO) (*67*). *Cd*HO exhibits significant sequence (*9*) and structural (*13, 16*) homology to hHO, in particular in the distal helix and the H-bond/ordered water molecule network (*18, 19*), with Tyr53, Arg132, Asp136, and Gly139 replacing Tyr58, Arg136, Asp140, and Gly143, respectively, and an ordered water molecule (water 1) similarly bridging the Asp136 carboxylate and exogenous ligand. However, the D136A-*Cd*HO mutant retains ~50% activity (*67*). Preliminary NMR evidence (not shown) suggests that the coupling between the exogenous ligand and homologous distal H-bond/ordered water network differs significantly between hHO and *Cd*HO; a more detailed comparative investigation of the hHO and *Cd*HO enzymes is in progress.

The NMR results for the hHO−DMDH−N_3 complex presented here indicate that the complex is primarily low-spin with a $(d_{xy})^2(d_{yz})^2(d_{xz})^1$ orbital ground state which is determined by the orientation of the ligated azide ion. The similarity of the substrate methyl contact shift patterns argues for a conserved $S = {}^1/_2$ ground state (with variable thermal occupation of the $S = {}^5/_2$ state) for the azide complexes of

[4] The D140A-hHO−DMDH−CN complex yields chemical shifts very similar to those of the WT hHO−DMDH−CN complex (*18*), with $1CH_3$, $2CH_3$, $3CH_3$, $4CH_3$, $5CH_3$, and $8CH_3$ shifts at 25 °C of 8.3, 20.0, 17.6, 7.6, 10.6, and 9.4 ppm for the former and 9.0, 21.3, 18.2, 8.5, 9.8, and 8.3 ppm for the latter, respectively.

the pathogenic bacterial HOs (*34*), with the orbital ground state determined by the proximal His ring orientation in the cyanide complexes (*22, 28*) and distal azide orientation in the azide complexes. Control of the orbital ground state in HOs by the azide ligand rather than by the axial His is attributed to a stronger ligand field by the azide in HOs versus that in globin complexes. This stronger azide axial field strength in HOs versus that in globins indicates weaker distal H-bonding to the ligand in HOs than in globins. The fact that this unusual orbital ground state is conserved in the inactive Asp140 → Ala mutant of hHO indicates that, while the novel orbital ground state may be characteristic of an orbital hole switch between the azide and cyanide all HO complexes, it simply reflects the relatively weak distal H-bonding to the ligand by an ordered water molecule and does not correlate with HO activity. Lastly, the proposed (*10, 34, 49*) weaker axial ligand field strength in azide-ligated HOs compared to azide-ligated globins that would stabilize a singly occupied d_{xy} orbital, which favors porphyrin ruffling that is key to the proposed free radical mechanism, is not supported by NMR data for HOs.

SUPPORTING INFORMATION AVAILABLE

One table and six figures (Curie plots for DMDH methyls in the hHO−DMDH−N_3 and D140A-hHO−DMDH−N_3 complexes, D140A-hHO−DMDH−N_3 spectra as a function of temperature, TOCSY spectra of paramagnetic and aliphatic residues in the hHO−DMDH−N_3 complex, and NOESY and TOCSY spectra for aromatic rings in the D140A-hHO−DMDH−N_3 complex). This material is available free of charge via the Internet at http://pubs.acs.org.

REFERENCES

1. Tenhunen, R., Marver, H. S., and Schmid, R. (1969) Microsomal heme oxygenase. Characterization of the enzyme. *J. Biol. Chem. 244*, 6388–6394.
2. Ortiz de Montellano, P. R., and Auclair, K. (2003) Heme Oxygenase Structure and Mechanism. In *The Porphryin Handbook* (Kadish, K. M., Smith, K. M., and Guilard, R., Eds.) pp 175−202, Elsevier Science, San Diego.
3. Unno, M., Matsui, T., and Ikeda-Saito, M. (2007) Structure and catalytic mechanism of heme oxygenase. *Nat. Prod. Rep. 24*, 553–570.
4. Stocker, R., Yamamoto, Y., McDonagh, A. F., Glazer, A. N., and Ames, B. N. (1987) Biliruben is an Antioxidant of Possible Physiological Importance. *Science 235*, 1043–1046.
5. Uzel, C., and Conrad, M. E. (1998) Absorption of heme iron. *Semin. Hematol. 35*, 27–34.
6. Baranano, D. E., and Snyder, S. H. (2001) Neural roles for heme oxygenase: Contrasts to nitric oxide synthase. *Proc. Natl. Acad. Sci. U.S.A. 98*, 10996–11002.
7. Beale, S. I. (1994) Biosynthesis of open-chain tetrapyrroles in plants, algae, and cyanobacteria. *Ciba Found. Symp. 180*, 156–168.
8. Wilks, A. (2002) Heme Oxygenase: Evolution, Structure, and Mechanism. *Antioxid. Redox Signaling 4*, 603–614.
9. Frankenberg-Dinkel, N. (2004) Bacterial Heme Oxygenases. *Antoxid. Redox Signaling 6*, 825–834.
10. Rivera, M., and Zeng, Y. (2005) Heme oxygenase, steering dioxygen activation toward heme hydroxylation. *J. Inorg. Biochem. 99*, 337–354.
11. Schuller, D. J., Wilks, A., Ortiz de Montellano, P. R., and Poulos, T. L. (1999) Crystal structure of human heme oxygenase-1. *Nat. Struct. Biol. 6*, 860–867.
12. Sugishima, M., Sakamoto, H., Higashimoto, Y., Omata, Y., Hayashi, S., Noguchi, M., and Fukuyama, K. (2002) Crystal structure of rat heme oxygenase-1 in complex with heme bound to azide: Implication for regiospecific hydroxylation of heme at the α-meso carbon. *J. Biol. Chem. 277*, 45086–45090.
13. Lad, L., Wang, J., Li, H., Friedman, J., Bhaskar, B., Ortiz de Montellano, P. R., and Poulos, T. L. (2003) Crystal Structures of the Ferric, Ferrous and Ferrous-NO Forms of the Asp140Ala Mutant of Human Heme Oxygenase-1: Catalytic Implications. *J. Mol. Biol. 330*, 527–538.
14. Sugishima, M., Sakamoto, H., Noguchi, M., and Fukuyama, K. (2003) Crystal Structures of CO-, CN-, and NO-Bound Forms of Rat Heme Oxygenase-1 (HO-1) in Complex with Heme: Structural Implications for Discrimination between CO and O_2 in HO-1. *Biochemistry 42*, 9898–9905.
15. Friedman, J., Lad, L., Li, H., Wilks, A., and Poulos, T. L. (2004) Structural Basis for Novel δ-Regioselective Heme Oxygenation in the Opportunistic Pathogen *Pseudomonas aeruginosa*. *Biochemistry 43*, 5239–5245.
16. Unno, M., Matsui, T., Chu, G. C., Coutoure, M., Yoshida, T., Rousseau, D. L., Olson, J. S., and Ikeda-Saito, M. (2004) Crystal Structure of the Dioxygen-bound Heme Oxygenase from *Corynebacterium diphtheriae*. *J. Biol. Chem. 279*, 21055–21061.
17. Friedman, J. M., Lad, L., Deshmukh, R., Li, H. Y., Wilks, A., and Poulos, T. L. (2003) Crystal structures of the NO- and CO-bound heme oxygenase from *Neisseriae meningitidis*: Implications for O_2 activation. *J. Biol. Chem. 278*, 34654–34659.
18. Li, Y., Syvitski, R. T., Auclair, K., Wilks, A., Ortiz de Montellano, P. R., and La Mar, G. N. (2002) Solution NMR characterization of an unusual distal H-bond network in the active site of the cyanide-inhibited, human heme oxygenase complex of the symmetric substrate, 2,4-dimethyldeuterohemin. *J. Biol. Chem. 277*, 33018–33031.
19. Li, Y., Syvitski, R. T., Chu, G. C., Ikeda-Saito, M., and La Mar, G. N. (2003) Solution ^{1}H NMR investigation of the active site molecular and electronic structures of the substrate-bound, cyanide-inhibited bacterial heme oxygenase from *C. diphtheriae*. *J. Biol. Chem. 279*, 6651–6663.
20. Li, Y., Syvitski, R. T., Auclair, K., Ortiz de Montellano, P. R., and La Mar, G. N. (2003) Solution ^{1}H, ^{15}N NMR spectroscopic characterization of substrate-bound cyanide-inhibited, human heme oxygenase: Water occupation of the distal cavity. *J. Am. Chem. Soc. 125*, 13392–13403.
21. Syvitski, R. T., Li, Y., Auclair, K., Ortiz de Montellano, P. R., and La Mar, G. N. (2002) ^{1}H NMR detection of immobilized water molecules within a strong hydrogen-bonding network in the distal side of substrate-bound human heme oxygenase. *J. Am. Chem. Soc. 124*, 14296–14297.
22. Liu, Y., Zhang, X., Yoshida, T., and La Mar, G. N. (2004) ^{1}H NMR characterization of the solution active site structure of substrate-bound, cyanide-inhibited heme oxygenase from *Neisseria meningitidis*: Comparison to crystal structures. *Biochemistry 43*, 10112–10126.
23. Ortiz de Montellano, P. R. (2000) The mechanism of heme oxygenase. *Curr. Opin. Chem. Biol. 4*, 221–227.
24. Wilks, A., and Demontellano, P. R. O. (1993) Rat Liver Heme Oxygenase: High Level Expression of a Truncated Soluble Form and Nature of the Meso-Hydroxylating Species. *J. Biol. Chem. 268*, 22357–22362.
25. Wilks, A., Torpey, J., and Ortiz de Montellano, P. R. (1994) Evidence for the electrophilic oxygen addition to the porphyrin ring in the formation of α-meso-hydroxyheme. *J. Biol. Chem. 269*, 29553–29556.
26. Wang, J., Evans, J. P., Ogura, H., La Mar, G. N., and Ortiz de Montellano, P. R. (2006) Alteration of the Regiospecificity of Human Heme Oxygenase-1 by Unseating of the Heme but not Disruption of the Distal Hydrogen Bonding Network. *Biochemistry 45*, 61–73.
27. Ogura, H., Evans, J. P., Ortiz de Montellano, P. R., and La Mar, G. N. (2008) Implication for Using Heme Methyl Hyperfine Shifts as Indicators of Heme Seating as Related to Stereoselectivity in the Catabolism of Heme by Heme Oxygenase: In-Plane Heme versus Axial His Rotation. *Biochemistry 47*, 421–430.
28. Caignan, G. A., Deshmukh, R., Wilks, A., Zeng, Y., Huang, H.-w., Moenne-Loccoz, P., Bunce, R. A., Eastman, M. A., and Rivera, M. (2002) Oxidation of heme to β- and δ-biliverdin by *Pseudomonas aeruginosa* Heme Oxygenase as a Consequence of an Unusual Seating of the Heme. *J. Am. Chem. Soc. 124*, 14879–14892.
29. Sharma, P. K., Kevorkiants, R., de Visser, S. P., Kumar, D., and Shaik, S. (2004) Porphyrin Traps Its Terminator! Concerted and Stepwise Porphyrin Degradation Mechanisms Induced by Heme-Oxygenase and Cytochrome P450. *Angew. Chem., Int. Ed. 43*, 1129–1132.

30. Kumar, D., de Visser, S. P., and Shaik, S. (2005) Theory Favors a Stepwise Mechanism of Porphyrin Degradation by a Ferric Hydroperoxide Model fo the Active Species of Heme Oxygenase. *J. Am. Chem. Soc. 127*, 8204–8213.
31. Chen, H., Moreau, Y., Derat, E., and Shaik, S. (2008) Quantum Mechanical/Molecular Mechanical Study of Mechanisms of Heme Degradation by the Enzyme Heme Oxygenase: The Strategic Function of the Water Cluster. *J. Am. Chem. Soc. 130*, 1953–1965.
32. Koenigs Lightning, L., Huang, H.-W., Moënne-Loccoz, P., Loehr, T. M., Schuller, D. J., Poulos, T. L., and Ortiz de Montellano, P. R. (2001) Disruption of an active site hydrogen bond converts human heme oxygenase-1 into a peroxidase. *J. Biol. Chem. 276*, 10612–10619.
33. Fujii, H., Zhang, X., Tomita, T., Ikeda-Saito, M., and Yoshida, T. (2001) A role for highly conserved carboxylate, aspartate-140, in oxygen activation and heme degradation by heme oxygenase-1. *J. Am. Chem. Soc. 123*, 6475–6484.
34. Zeng, Y., Caignan, G. A., Bunce, R. A., Rodriguez, J. C., Wilks, A., and Rivera, M. (2005) Azide-inhibited Bacterial Heme Oxygenases Exhibit an S=3/1 $(d_{xz},d_{yz})3(d_{xy})^1(d_z^2)^1$ Spin State: Mechanistic Implications for Heme Oxidation. *J. Am. Chem. Soc. 127*, 9794–9807.
35. Ma, L.-H., Liu, Y., Zhang, X., Yoshida, T., and La Mar, G. N. (2009) ^{1}H NMR study of the effect of variable ligand on heme oxygenase electronic and molecular structure. *J. Inorg. Biochem. 103*, 10–19.
36. Yoshida, T., Noguchi, M., and Kikuchi, G. (1980) Oxygenated Form of Heme-Heme Oxygenase Complex and Requirement for Second Electron to Initiate Heme Degradation from the Oxygenated Complex. *J. Biol. Chem. 255*, 4418–4420.
37. Sun, J., Wilks, A., Ortiz de Montellano, P. R., and Loehr, T. M. (1993) Resonance Raman and EPR Spectroscopic Studies on Heme Heme Oxygenase Complexes. *Biochemistry 32*, 14151–14157.
38. Takahashi, S., Wang, J. L., Rousseau, D. L., Ishikawa, K., Yoshida, T., Takeuchi, N., and Ikeda-Saito, M. (1994) Heme-Heme Oxygenase Complex: Structure and Properties of the Catalytic Site from Resonance Raman Scattering. *Biochemistry 33*, 5531–5538.
39. Chu, G. C., Tomita, T., Sönnichsen, F. D., Yoshida, T., and Ikeda-Saito, M. (1999) The heme complex of Hmu O, a bacterial heme degradation enzyme from *Corynebacterium diphtheriae*. *J. Biol. Chem. 274*, 24490–24496.
40. Hernández, G., Wilks, A., Paolesse, R., Smith, K. M., Ortiz de Montellano, P. R., and La Mar, G. N. (1994) Proton NMR Investigation of Substrate-bound Heme Oxygenase: Evidence for Electronic and Steric Contributions to Stereoselective Heme Cleavage. *Biochemistry 33*, 6631–6641.
41. Gorst, C. M., Wilks, A., Yeh, D. C., Ortiz de Montellano, P. R., and La Mar, G. N. (1998) Solution ^{1}H NMR investigation of the molecular and electronic structure of the active site of substrate-bound human heme oxygenase: The nature of the distal hydrogen bond donor to bound ligands. *J. Am. Chem. Soc. 120*, 8875–8884.
42. La Mar, G. N., Satterlee, J. D., and de Ropp, J. S. (2000) NMR of Hemoproteins. In *The Porphyrins Handbook* (Kadish, K. M., Smith, K. M., and Guilard, R., Eds.) pp 185−298, Academic Press, San Diego.
43. Bertini, I., and Luchinat, C. (1996) NMR of Paramagnetic Substances. *Coord. Chem. Rev. 150*, 1–296.
44. Shokhirev, N. V., and Walker, F. A. (1998) The Effect of Axial Ligand Plane Orientation on the Contact and Pseudocontact Shifts of Low-spin Ferriheme Proteins. *J. Biol. Inorg. Chem. 3*, 581–594.
45. Walker, F. A. (2000) Proton NMR and EPR Spectroscopy of Paramagnetic Metalloporphyrin. In *The Porphyrin Handbook* (Kadish, K. M., Smith, K. M., and Guilard, R., Eds.) pp 1−183, Academic Press, San Diego.
46. Liu, Y., Ma, L.-H., Zhang, X., Yoshida, T., Satterlee, J. D., and La Mar, G. N. (2006) ^{1}H NMR study of the influence of hemin vinyl-methyl substitution on the interaction between the C-terminus and substrate and the "aging" of the heme oxygenase from *N. meningitidis*. Induction of active site structural heterogeneity by a two-fold symmetric hemin. *Biochemistry 45*, 13875–13888.
47. Zhu, W., Li, Y., Wang, J., Ortiz de Montellano, P. R., and La Mar, G. N. (2006) Solution NMR study of environmental effects on substrate seating in human heme oxygenase: Influence of polypeptide truncation, substrate modification and axial ligand. *J. Inorg. Biochem. 100*, 97–107.
48. La Mar, G. N., Asokan, A., Espiritu, B., Yeh, D. C., Auclair, K., and Ortiz de Montellano, P. R. (2001) Solution ^{1}H NMR of the active site of substrate-bound, cyanide-ligated, human heme oxygenase. Comparison to the crystal structure of the water-ligated form. *J. Biol. Chem. 276*, 15676–15687.
49. Caignan, G. A., Deshmukh, R., Zeng, Y., Wilks, A., Bunce, R. A., and Rivera, M. (2003) The Hydroxide Complex of *Pseudomonas aeruginosa* Heme Oxygenase as a Model of the Low-Spin Iron(III) Hydroperoxide Intermediate in Heme Catabolism: ^{13}C NMR Spectroscopic Studies Suggest the Active Participation of the Heme in Macrocycle Hydroxylation. *J. Am. Chem. Soc. 125*, 11842–11852.
50. Smith, K. M., and Kehres, L. A. (1983) Syntheses of Methyl Devinylporphyrins Related to Protoporphyrin-IX. Initial Studies on the Mechanism of the Copper (II) Catalyzed Cyclizations of 1′,8′-Dimethyl-a,c-biladienes. *J. Chem. Soc., Perkin Trans. 1*, 2329–2335.
51. Jeener, J., Meier, B. H., Bachmann, P., and Ernst, R. R. (1979) Investigation of Exchange Processes by Two Dimensional NMR Spectroscopy. *J. Chem. Phys. 71*, 4546–4553.
52. Griesinger, C., Otting, G., Wüthrich, K., and Ernst, R. R. (1988) Clean TOCSY for ^{1}H Spin System Identification in Macromolecules. *J. Am. Chem. Soc. 110*, 7870–7872.
53. Evans, D. F. (1959) The determination of the paramagnetic susceptibility of substances in solution by nuclear magnetic resonance. *J. Chem. Soc.,* 2003–2005.
54. Bertini, I., Luchinat, C., Turano, P., Battaini, G., and Casella, L. (2003) The Magnetic Properties of Myoglobin as Studied by NMR Spectroscopy. *Chem.−Eur. J. 9*, 2316–2322.
55. Sandström, J. (1982) *Dynamic NMR Spectroscopy*, Academic Press, New York.
56. Lad, L., Schuller, D. J., Shimizu, H., Friedman, J., Li, H., Ortiz de Montellano, P. R., and Poulos, T. L. (2003) Comparison of the Heme-free and -bound Crystal Structures of Human Heme Oxygenase-1. *J. Biol. Chem. 278*, 7834–7843.
57. Banci, L., Bertini, I., and Luchinat, C. (1991) *Nuclear and electronic relaxation*, VCH, Weinheim, Germany.
58. Iizuka, T., and Kotani, M. (1969) Analysis of thermal equilibrium between high-spin and low-spin states in ferrimyoglobin complexes. *Biochim. Biophys. Acta 181*, 275–286.
59. Iizuka, T., and Morishima, I. (1974) 220 MHz Proton NMR Studies of Hemoproteins High-spin−Low-spin Equilibrium in Ferric Myoglobin and Hemoglobin Derivatives. *Biochim. Biophys. Acta 371*, 1–13.
60. Ikeda-Saito, M., and Fujii, H. (2003) EPR Characterization of the Heme Oxygenase Reaction Intermediates and Its Implication for the Catalytic Mechanism. In *Paramagnetic Resonance of Metallobiomolecules* (Tesler, J., Ed.) pp 97−112, Oxford University Press, New York.
61. Takahashi, S., Wang, J., Rousseau, D. L., Ishikawa, K., Yoshida, T., Host, J. R., and Ikeda-Saito, M. (1994) Heme-Heme Oxygenase Complex Structure of the Catalytic Site and Its Implication for Oxygen Activation. *J. Biol. Chem. 269*, 1010–1014.
62. Sugishima, M., Sakamoto, H., Kakuta, Y., Omata, Y., Hayashi, S., Noguchi, M., and Fukuyama, K. (2002) Crystal Structue of Rat Apo-Heme Oxygenase-1 (HO-1): Mechanism of Heme Binding in HO-1 Inferred from Structural Comparison of the Apo and Heme Complex Forms. *Biochemistry 41*, 7293–7300.
63. Springer, B. A., Sligar, S. G., Olson, J. S., and Phillips, G. N. (1994) Mechanisms of Ligand Recognition in Myoglobin. *Chem. Rev. 94*, 699–714.
64. Davydov, R. M., Yoshida, T., Ikeda-Saito, M., and Hoffman, B. M. (1999) Hydroperoxy-Heme Oxygenase Generated by Cryoreduction Catalyzes the Formation of α-*meso*-Hydroxyheme as Detected by EPR and ENDOR. *J. Am. Chem. Soc. 121*, 10656–10657.
65. Wojciechowski, G., and Ortiz de Montellano, P. R. (2007) Radical Energies and the Regiochemistry of Addition to Heme Groups. Methylperoxy and Nitrite Radical Additions to the Heme of Horseradish Peroxidase. *J. Am. Chem. Soc. 129*, 1663–1672.
66. Rivera, M., Caignan, G. A., Astashkin, A. V., Raitsimring, A. M., Shokhireva, T. K., and Walker, F. A. (2002) Models of the Low-Spin Iron(III) Hydroperoxide Intermediate of Heme Oxygenase: Magnetic Resonance Evidence for Thermodynamic Stabilization of the d_{xy} Electronic State at Ambient Temperature. *J. Am. Chem. Soc. 124*, 6077–6089.
67. Matsui, T., Furukawa, M., Unno, M., Tomita, T., and Ikeda-Saito, M. (2005) Roles of Distal Asp in Heme Oxygenase from *Corynebacterium diphtheriae*, HmuO. *J. Biol. Chem. 280*, 2981–2989.

BI802360G